# Electrically Tunable Terahertz Resonance in Antiferromagnetic NiO/Pt Heterostructures

Dongsheng Yang[1,†], Wen Wen[2,†], Chang Xu[1,†], Kyusup Lee[1], Ting Yu[2], and Hyunsoo Yang[1,*]

[1]*Department of Electrical and Computer Engineering, National University of Singapore, Singapore 117576, Singapore*

[2]*Division of Physics and Applied Physics, School of Physical and Mathematical Sciences, Nanyang Technological University, Singapore 637371, Singapore*

Antiferromagnets that facilitate terahertz (THz) spin resonances have the potential to revolutionize high-speed electronics at the nanoscale. The electrical control of THz spin resonances is the key to such THz devices; however, experimental demonstration has remained elusive. In this work, we demonstrate electrically tunable THz spin resonance in an antiferromagnetic NiO/Pt heterostructure by employing both low-wavenumber Raman and continuous-wave THz spectroscopy techniques. A redshift of over 100 GHz in the NiO spin resonance frequency of around 1 THz is observed by applying charge currents along the adjacent Pt layer. A control experiment with NiO/Cu and temperature-dependent measurement confirm that the dominant tuning mechanism is Joule heating. Finally, a prototype device is designed to achieve an electrical control of THz transmission at dual channels of 0.96 and 1 THz, leading to a $Q$ factor of 56. This work opens up the possibility for the implementation of tunable THz devices utilizing antiferromagnetic spin resonance.

## I. INTRODUCTION

Antiferromagnetism is a type of magnetism with opposing magnetic moments between neighboring sublattices. It has recently gained much attention in the field of terahertz (THz) spintronics due to its unique electrical and magnetic properties in the THz range [1]. For example, it hosts intrinsic THz-speed spin dynamics such as collective spin resonances [2,3], and these dynamical properties are highly susceptible to various external stimuli such as magnetic field [4], strain [5], temperature [6], doping [7], current [8,9], electric field [10], and light [11,12]. These advantages make an antiferromagnet a key material for realizing high-performance tunable THz devices such as on-chip THz sources [13].

Nickel oxide (NiO) is a well-studied prototype antiferromagnetic insulator with a rock-salt crystal structure [2,14–18]. NiO is a charge-transfer insulator for which both the long-range magnetic ordering and the insulating behavior are mediated by local electron correlations via the Anderson superexchange mechanism [17,19], leading to antiferromagnetism and a wide band gap $E_g$ of 4 eV below the Néel temperature $T_N$ of 523 K [20]. In the antiferromagnetic phase (below $T_N$), the $Ni^{2+}$ electron spins

are aligned in parallel within (111) planes and antiparallel with neighboring (111) planes, resulting in a zero net magnetic moment as illustrated in Fig. 1(a). NiO is chosen in this work because it possesses high-frequency spin resonances at 1 THz and its strongly correlated electrons provide an additional tunability. In addition, the high $T_N$ of NiO facilitates practical applications at room temperature.

Thus far, various approaches such as the use of pressure [21], magnetic field [4], and cation substitution [7] have been developed to control the spin resonance in NiO. The limitations of previous approaches are that they are difficult to change or scale down once implemented. To satisfy the demands of high-speed nanointegrated devices, it is desired to control the THz spin resonance using a current input. Although there are theoretical reports on electrically tuning the spin resonance frequency in antiferromagnets by using spin-orbit torques, an experimental demonstration remains still elusive.

In this work, we demonstrate in an antiferromagnetic NiO/Pt heterostructure in which the spin resonance frequency ($f_r$) of NiO is actively tuned by applying charge currents along the adjacent metallic Pt layer at a frequency of 1 THz. The result shows that $f_r$ in NiO redshifts monotonically with the application of current density ($J_c$) up to $5.6 \times 10^7$ A cm$^{-2}$. We further distinguish that the dominant $f_r$ tuning mechanism is current-induced Joule heating through NiO/Cu control devices and

---

*eleyang@nus.edu.sg
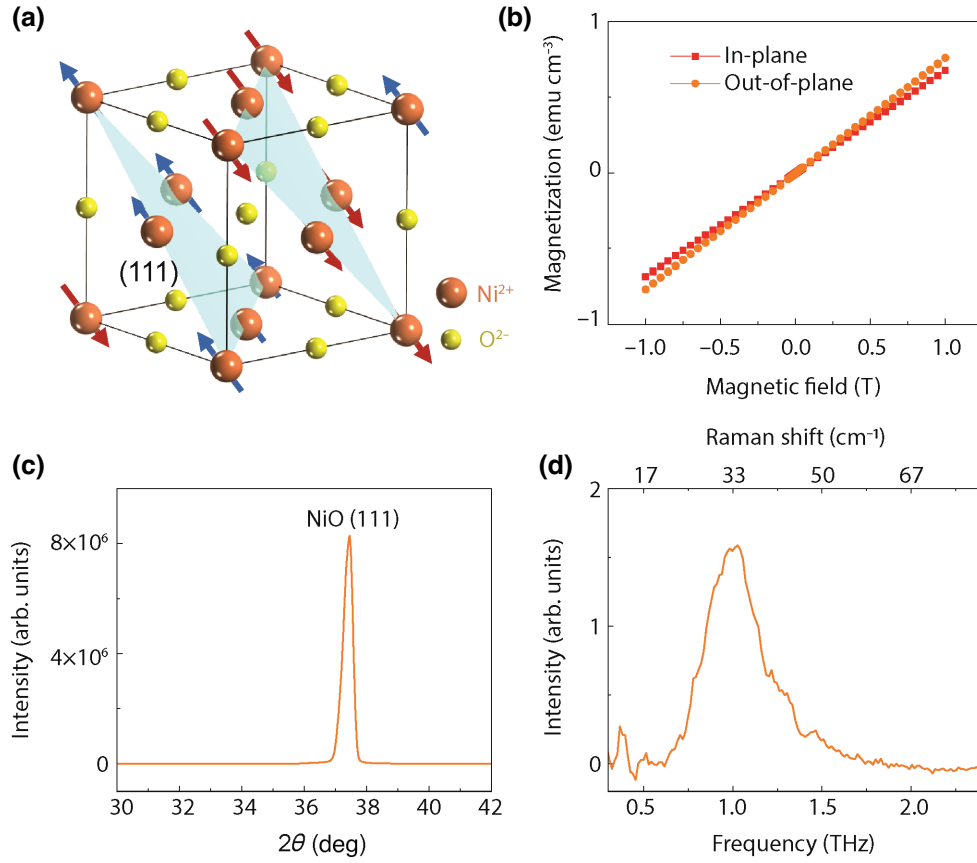†These authors contributed equally to this work.

FIG. 1.    (a) Illustration of NiO crystalline and magnetic structure. (b) Vibrating sample magnetometry results of NiO(111) sample. The absence of a hysteresis loop confirms the compensated antiferromagnetic phase of NiO. (c) X-ray diffraction results of NiO crystal. The single peak observed at 37.5° with a narrow linewidth indicates a good crystal quality of NiO(111) orientation. (d) 1 THz (33 cm$^{-1}$) spin resonance mode is observed in NiO by using low-wavenumber Raman spectroscopy.

temperature-dependent $f_r$ measurement. Finally, we utilize this mechanism to construct a prototype device for actively tuning the transmission of continuous-wave THz (cw-THz) radiation around 1 THz.

## II. RESULTS AND DISCUSSION

We first characterize the crystalline and magnetic properties of NiO(111) crystal by using vibrating sample magnetometry (VSM) and x-ray diffraction (XRD) techniques. Figure 1 summarizes the characterization results. A commercially available single-crystal NiO(111) slat with dimensions of 5 mm long × 5 mm wide × 1 mm thick is used in this work for both spin resonance characterization and THz device fabrication. We employ a 1-mm-thick NiO sample due to the direct correlation between THz absorption and sample thickness, making it an ideal choice for prototypical demonstrations of the THz tuning experiment. Furthermore, the thin-film-based NiO sample exhibits magnetic domain sizes typically on the micrometer scale, rendering it unsuitable for achieving the desired optimized signal [22]. The VSM results of the NiO crystal

along (in plane) and perpendicular to (out of plane) the [111] direction are shown in Fig. 1(b). The absence of a ferromagnetic hysteresis loop confirms the pure compensated antiferromagnetic phase in our NiO sample. XRD results in Fig. 1(c) show a single peak at 37.5°, indicating a good crystalline quality of NiO(111).

To investigate the electrically tunable spin resonance in NiO, Raman spectra are collected with a low-wavenumber confocal microscopic Raman system (WeTec Alpha 300). A 532-nm continuous-wave laser is harnessed to excite the sample and Raman signals are collected with a 50× objective lens (NA = 0.55). The estimated probing length for NiO/Pt (5 nm) is approximately 25 μm. The cross-polarization (*XY*) configuration is employed to maximize the spin-origin signal component. The $f_r$ of antiferromagnets can be extracted from the two-sublattice coupled Landau-Lifshitz-Gilbert equations based on the Kittel theory [23]:

$$f_r = \frac{\gamma}{2\pi}\sqrt{2H_E H_A}, \tag{1}$$

where $\gamma = 1.76 \times 10^{11}$ T$^{-1}$ s$^{-1}$ is the electron gyromagnetic ratio and $H_E$ and $H_A$ indicate the effective exchange field and magnetic anisotropy field, respectively. Since the typical value of $H_E \sim 1000$ T is much larger than that of $H_A \sim 1$ T in antiferromagnets, $H_E$ amplifies $f_r$ to THz frequencies, which are 2 to 3 orders of magnitude higher than those of their ferromagnetic counterparts. In NiO, there is a three-fold symmetric easy-axis magnetic anisotropy in the (111) plane and a hard-axis magnetic anisotropy along the [111] direction, leading to two spin resonance modes such as the low-frequency mode ($f_L = 0.13$ THz) and high-frequency mode ($f_H = 1$ THz) [9,18]. A representative Raman spectrum peak of 1 THz in Fig. 1(d) shows a good agreement with the high-frequency mode in NiO.

To prepare a device for applying $J_c$, a layer of negative photoresist (PFI) is spin-coated and the patterning of the device is completed using a mask-free photolithography system (TTT-07-UVlitho, Tuotuo Tech. Ltd). Afterward, a 5-nm-thick metal layer (Pt or Cu) and a 4-nm-thick capping layer (SiO$_2$) are deposited using magnetron sputtering with a base pressure of less than $2 \times 10^{-9}$ Torr (ATC, AJA Int. Ltd). The channel size of the device is 10 μm long and 5 μm wide. As illustrated in Fig. 2(a), the Raman measurements are performed with a laser spot on the center of the device channel. Direct currents are applied to tune $f_r$ of the NiO spin resonance during the Raman measurement.

Figure 2(b) shows the Raman spectra of NiO(111)/Pt(5 nm)/SiO$_2$(4 nm) (for brevity, NiO/Pt is used in the following text) under the various $J_c$ along the adjacent Pt channel. It is seen that $f_r$ is monotonically redshifted with increasing $J_c$. As shown in Fig. 2(b), without the current, $f_r$ of NiO is found to be around 1.04 THz. On the contrary, at $J_c = 5.1 \times 10^7$ A cm$^{-2}$, $f_r$ decreases to 0.91 THz, leading to a frequency tunability ($\eta$) of 12.5%. We notice that this $\eta$ is comparable to previously reported values through cation substitution [7] and pressure [21] but much easier to implement for functional devices.

In addition, we note that the spin resonance mode is split into two branches at high $J_c$, which is noticeable when $J_c \geq 3.2 \times 10^7$ A cm$^{-2}$ in Fig. 2(b). We attribute this splitting to a result of the surface magnon mode [25] or a combined effect among the superexchange interaction, dipolar coupling, and small cubic anisotropy [26]. However, the broad branch ($<0.9$ THz) of the spin resonance mode, on the other hand, is absent in the THz-wave transmission measurements as discussed later. It shows that the broad branch is insensitive to transmitted THz radiation, thereby unsuitable for THz tuning applications.

The redshift of the spin resonance can be attributed either to the current-induced spin-orbit torque [24] or, indirectly, to the effects of current-induced heating and strain. Specifically, in the case of NiO, both spin-orbit torque and heating contribute to a redshift in the spin resonance frequency. To investigate the $f_r$ tuning mechanism

in NiO/Pt in Fig. 2(c), we also measure the spin resonance in NiO(111)/Cu(5 nm)/SiO$_2$(4 nm) (referred as NiO/Cu in the following text) as shown in Fig. 2(d). This is because while Pt has strong spin-orbit coupling and a corresponding large spin-orbit torque on an adjacent magnetic layer, Cu is known to have negligible spin-orbit coupling as well as small spin-orbit torques [27]. Therefore, a comparative study of Pt and Cu with currents enables one to distinguish the spin current effect from heating effects. The $f_r$ of NiO/Cu presents the same decreasing trend with increasing $J_c$ similar to the NiO/Pt case in Fig. 2(c). Therefore, we can exclude the spin current or spin-orbit torque as the dominant $f_r$ tuning mechanism for both the Pt and Cu cases. The frequency changes of $f_r$ at $J_c = 5 \times 10^7$ A cm$^{-2}$ compared with that without currents for NiO/Pt and NiO/Cu devices are 0.11 and 0.12 THz, respectively. We note that the ratio of $f_r$ change, $0.11/0.12 = 0.917$, is close to the ratio of device resistance ($R$), 0.934 using $R_{\text{NiO/Pt}} = 496$ Ω and $R_{\text{NiO/Cu}} = 531$ Ω. This result follows from the dissipated Joule heating being proportional to the resistance and therefore strongly supports the fact that current-induced Joule heating plays a major role in tuning $f_r$. To further confirm, temperature-dependent measurements of the NiO/Pt device are performed. Monotonically decreasing $f_r$ with increasing temperature $T$ is observed between 300 and 380 K as shown in Fig. 2(e). The current-induced local temperature rise $\Delta T$ is evaluated from the Pt resistance [28]. $\Delta T \sim 40$ K at $J_c = 5.6 \times 10^7$ A cm$^{-2}$ matches well with the temperature-dependent $f_r$ trend in Fig. 2(e), confirming that the current-induced Joule heating is the dominant $f_r$ tuning mechanism in this work. While the thermal-induced redshift of the spin resonance is present, it is unable to completely compensate for the magnetic damping, thereby preventing the attainment of self-oscillation, in contrast to the effects of spin-orbit torques. Moreover, at the Curie temperature, the spin resonance frequency is expected to approach zero due to the disappearance of long-range magnetic ordering.

Furthermore, we calculate the frequency change induced by the spin-orbit torque effect [24] with reported NiO parameters: sublattice magnetization $M_s = 380$ kA/m, exchange field $H_{\text{ex}} = 1000$ T, and anisotropy field $H_{\text{ani}} = 0.61$ T [6]. As shown by the gray line of Fig. 2(c), the frequency change is within 5 GHz under $J_c = 6 \times 10^7$ A cm$^{-2}$. This is due to the large $H_{\text{ani}}$ of NiO that reduces the tuning efficiency of spin-orbit torques, confirming that the dominant tuning mechanism of our observation is the current-induced Joule heating effect. Besides, Fig. 3(a) shows the linewidth of spin resonance with $J_c$ extracted from Fig. 2(b). The monotonically increasing linewidth with increasing $J_c$ is distinct from the theoretically predicted trend due to spin-orbit torques, in which the linewidth should be independent of the current.
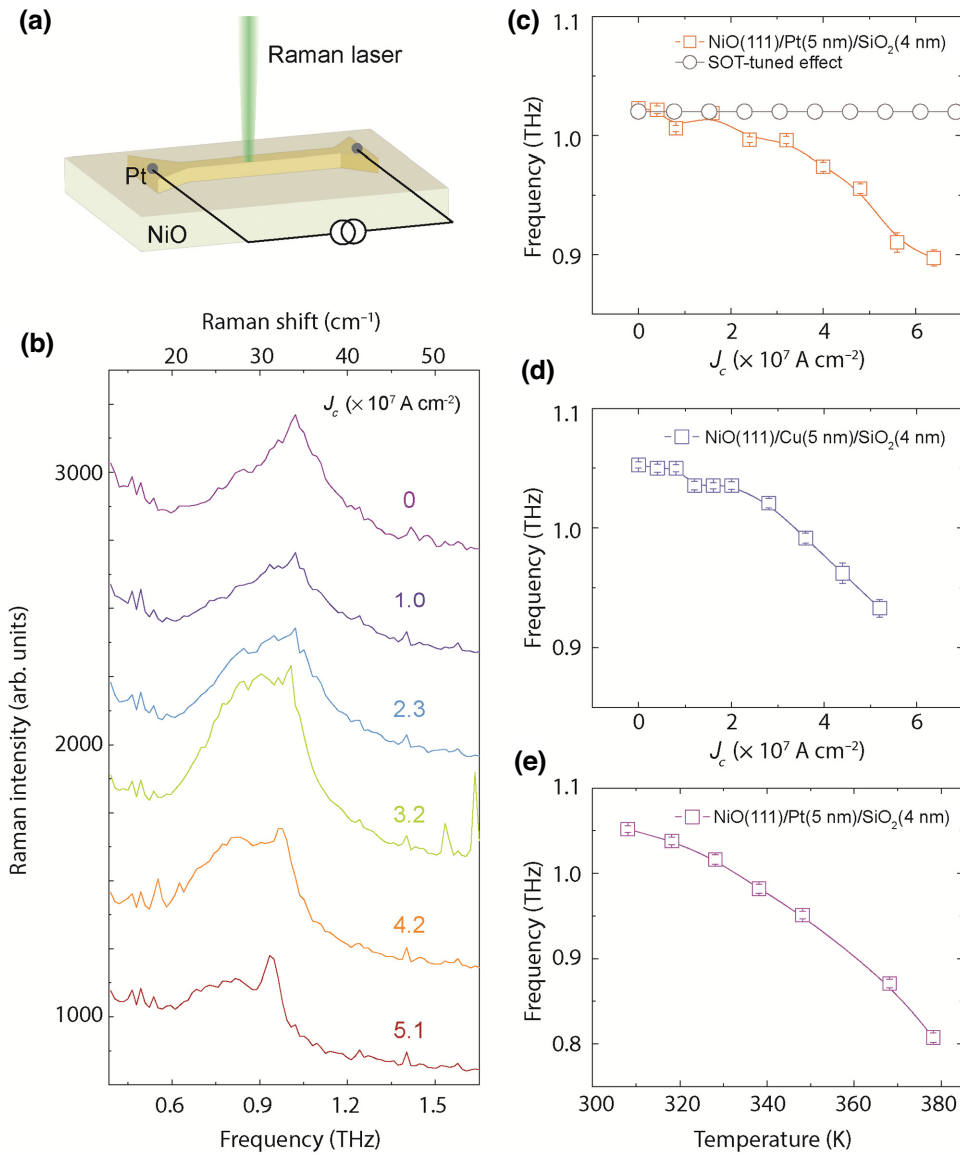
FIG. 2. (a) Measurement scheme of electrically tunable THz resonance in NiO/Pt(5 nm) heterostructure. Charge currents are applied along the adjacent Pt layer to interplay with adjacent NiO, thus affecting the THz resonance frequency in NiO. (b) Raman spectra of NiO(111)/Pt(5 nm)/SiO$_2$(4 nm) with increasing the current density ($J_c$). Vertical offsets are applied for clarity. (c) Spin resonance frequency ($f_r$) versus $J_c$ for NiO(111)/Pt(5 nm)/SiO$_2$(4 nm). The gray line indicates the calculated frequency change due to the spin-orbit torque effect according to Ref. [24]. (d) $f_r$ vs $J_c$ in NiO(111)/Cu(5 nm)/SiO$_2$(4 nm). (e) The temperature-dependent $f_r$ in NiO(111)/Pt(5 nm)/SiO$_2$(4 nm) device.

To distinguish the current-induced strain effect and heating effect in NiO/Pt, we measure the spin resonance frequency using a cross-shaped NiO/Pt(5 nm) device with $J_c$ along two perpendicular lattice crystal directions [see the inset of Fig. 3(b)]. In contrast to the heating effect, the current-induced strain effect on spin resonance is quite sensitive to the crystal orientation. This sensitivity arises from the deformation of the lattice structure, leading to distinct responses expected for different $J_c$ directions [5]. However, as depicted in Fig. 3(b), it is evident that the

spin resonance frequency decreases uniformly when $J_c$ is applied along either direction. This observation indicates that our tuning mechanism is independent of the crystalline direction, thus ruling out the possibility of a strain effect. This outcome is reasonable, considering that the maximum applied current density ($6.4 \times 10^7$ A cm$^{-2}$) in our study is less than half of the critical current density ($1.95 \times 10^8$ A cm$^{-2}$) required to observe a noticeable strain effect, as reported in Ref. [16]. Hence, in our NiO sample, the current-induced heating effect proves to
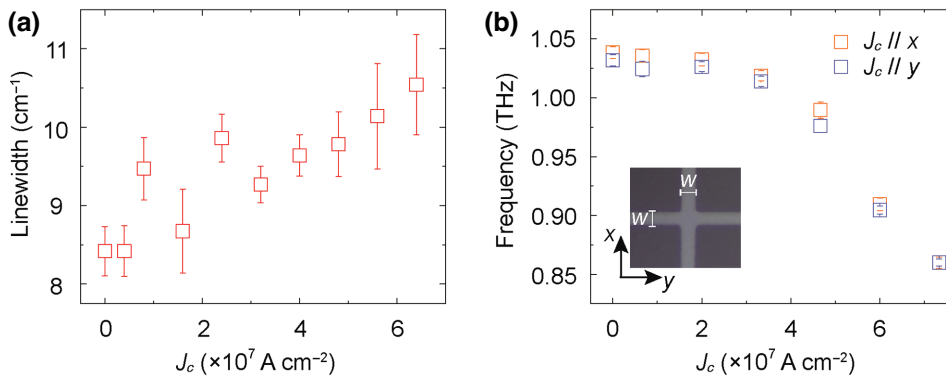
FIG. 3.   (a) The linewidth of spin resonance as a function of $J_c$ for NiO(111)/Pt(5 nm)/SiO$_2$(4 nm) device. (b) The spin resonance frequency with $J_c$ applied along two perpendicular crystal directions. The inset is an image of the cross-shaped NiO/Pt(5 nm) device with a channel width of $W = 6$ μm.

be the more dominant factor in tuning the spin resonance.

Finally, we construct a prototype device with a channel size of 2 mm in width, 5 mm in length, and 3 nm in thickness of Pt, aiming at a proof-of-concept demonstration of tunable cw-THz transmission using antiferromagnetic spin resonances. As shown in Fig. 4(a), a photomixer-based cw-THz system (TeraScan 1550, Toptica Ltd) is used for

both single-frequency cw-THz generation and detection. We define 0.96 and 1 THz as two independent THz information channel 1 and channel 2, respectively. As shown by the blue line in Fig. 4(b), channel 2 (1 THz) is blocked in the absence of $J_c$ due to the enhanced absorption of NiO spin resonance, which is defined as the "off" state. The baseline of the Fabry-Perot effect is subtracted by using the inverse Fourier transform in the time domain for clarity. By applying $J_c = 1.7 \times 10^7$ A cm$^{-2}$, $f_r$ is redshifted to the frequency of channel 1 (0.96 THz) and thereby the transmitted THz signal in channel 2 is enhanced from below 10 to 50 μV, switching channel 2 to the "on" state. Conversely, channel 1 is turned "off" accordingly. Figure 5 illustrates the electrical tunability of THz waves at both 0.96 and 1 THz with currents. We note that the thermal-effect-based control technique is not inherently slow. For example, ultrafast heating can be achieved on picosecond timescales using ultrafast optical techniques [29].

To evaluate the device performance, the quality factor ($Q$ factor) of our prototype NiO device is extracted from the resonance linewidth $\Delta f$ :

$$Q = \frac{f_r}{\Delta f}. \tag{2}$$

The $Q$ factor of our prototype device is 56. Although this is a prototype device without much optimization, the performance is comparable with the recently reported high $Q$ of 68 in a THz metasurface [30]. This is due to the inherent low magnetic dissipation in NiO. Another advantage is that this scheme does not require any complex artificial structures, allowing the scaling of the device to the nanoscale. For example, the dimensions of other terahertz devices such as photonic crystals, metasurfaces and THz waveguides are typically limited to tens of micrometers [31,32]. Notably, our device size ($5 \times 10$ μm$^2$) used for the electrically tuned THz resonance in Raman measurements is 1–2 orders smaller than that of other approaches. These results suggest that the method of tunable THz spin resonance is well suited for developing tunable THz filters, despite the simplicity of the underlying concept. Recent experimental reports [33,34] have further demonstrated that robust THz
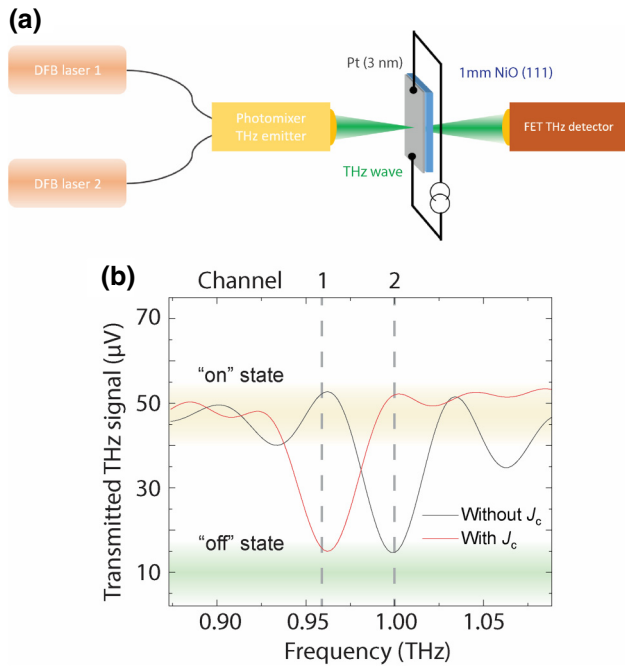


FIG. 4.   (a) Tunable THz transmission measurement of NiO/Pt device by using a cw-THz system. The experimental design of cw-THz measurement based on a THz photomixer setup. The cw-THz beam is generated at a photomixer by a heterodyne technique with two distributed feedback (DFB) lasers and detected by a home-made field-effect transistor (FET) THz detector. (b) Frequency-dependent THz transmission of NiO/Pt device. The transmission dip indicates enhanced THz absorption at the NiO spin resonance frequency. The background of multiple reflections (the Fabry-Perot effect) is subtracted in the time domain by using the inverse Fourier transform.
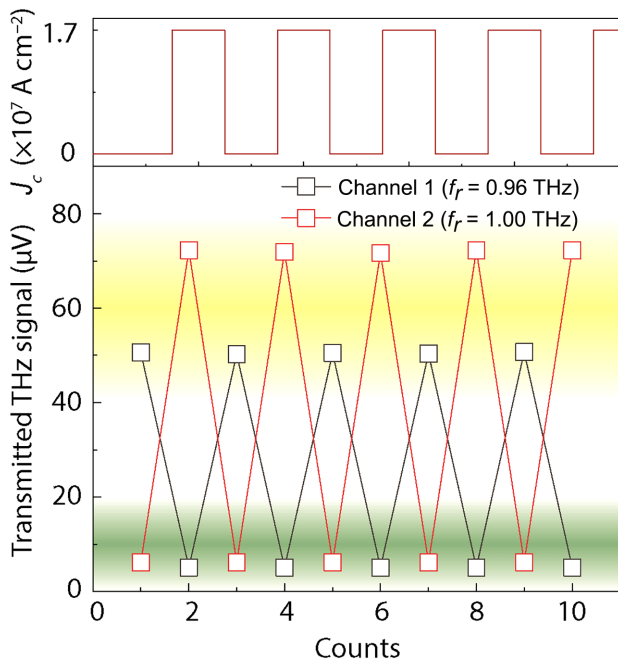
FIG. 5.　Tunable THz transmission of the NiO/Pt device at 0.96 THz (black symbols) and 1 THz (red symbols).

spin resonances occur on sub-100-nm-thick NiO films, showing the tantalizing promise of nanosize on-chip THz communication with this novel scheme.

## III. CONCLUSION

We demonstrate electrically tunable THz spin resonance in NiO/Pt antiferromagnetic heterostructures using Raman and continuous-wave THz techniques. We observe a significant redshift of 100 GHz in the NiO spin resonance frequency around 1 THz when a current density of $5.1 \times 10^7$ A cm$^{-2}$ is applied along the adjacent Pt layer, with Joule heating being the dominant frequency tuning mechanism. We also design a prototype device that demonstrates electrical tuning of cw-THz transmission with a high $Q$ factor of 56. We believe that our work provides additional possibilities for electrical control of THz transmission, thereby facilitating antiferromagnets for applications in THz communication.

---

[1] T. Jungwirth, X. Marti, P. Wadley, and J. Wunderlich, Antiferromagnetic spintronics, Nat. Nanotechnol. **11**, 231 (2016).

[2] T. Kampfrath, A. Sell, G. Klatt, A. Pashkin, S. Mährlein, T. Dekorsy, M. Wolf, M. Fiebig, A. Leitenstorfer, and R. Huber, Coherent terahertz control of antiferromagnetic spin waves, Nat. Photonics **5**, 31 (2011).

[3] A. Kimel, A. Kirilyuk, A. Tsvetkov, R. Pisarev, and T. Rasing, Laser-induced ultrafast spin reorientation in the antiferromagnet TmFeO$_3$, Nature **429**, 850 (2004).

[4] Z. Wang, S. Kovalev, N. Awari, M. Chen, S. Germanskiy, B. Green, J.-C. Deinert, T. Kampfrath, J. Milano, and M. Gensch, Magnetic field dependence of antiferromagnetic resonance in NiO, Appl. Phys. Lett. **112**, 252404 (2018).

[5] H.-H. Kim, K. Ueda, S. Nakata, P. Wochner, A. Mackenzie, C. Hicks, G. Khaliullin, H. Liu, B. Keimer, and M. Minola, Giant stress response of terahertz magnons in a spin-orbit Mott insulator, Nat. Commun. **13**, 6674 (2022).

[6] T. Moriyama, K. Hayashi, K. Yamada, M. Shima, Y. Ohya, and T. Ono, Intrinsic and extrinsic antiferromagnetic damping in NiO, Phys. Rev. Mater. **3**, 051402 (2019).

[7] T. Moriyama, K. Hayashi, K. Yamada, M. Shima, Y. Ohya, and T. Ono, Tailoring THz antiferromagnetic resonance of NiO by cation substitution, Phys. Rev. Mater. **4**, 074402 (2020).

[8] R. Khymyn, I. Lisenkov, V. Tiberkevich, B. A. Ivanov, and A. Slavin, Antiferromagnetic THz-frequency Josephson-like oscillator driven by spin current, Sci. Rep. **7**, 43705 (2017).

[9] R. Cheng, D. Xiao, and A. Brataas, Terahertz Antiferromagnetic Spin Hall Nano-oscillator, Phys. Rev. Lett. **116**, 207603 (2016).

[10] X.-X. Zhang, L. Li, D. Weber, J. Goldberger, K. F. Mak, and J. Shan, Gate-tunable spin waves in antiferromagnetic atomic bilayers, Nat. Mater. **19**, 838 (2020).

[11] R. Mikhaylovskiy, E. Hendry, A. Secchi, J. H. Mentink, M. Eckstein, A. Wu, R. Pisarev, V. Kruglyak, M. Katsnelson, T. Rasing, and A. Kimel, Ultrafast optical modification of exchange interactions in iron oxides, Nat. Commun. **6**, 8190 (2015).

[12] D. Afanasiev, J. Hortensius, B. Ivanov, A. Sasani, E. Bousquet, Y. Blanter, R. Mikhaylovskiy, A. Kimel, and A. Caviglia, Ultrafast control of magnetic interactions via light-driven phonons, Nat. Mater. **20**, 607 (2021).

[13] V. Baltz, A. Manchon, M. Tsoi, T. Moriyama, T. Ono, and Y. Tserkovnyak, Antiferromagnetic spintronics, Rev. Mod. Phys. **90**, 015005 (2018).

[14] T. Satoh, S.-J. Cho, R. Iida, T. Shimura, K. Kuroda, H. Ueda, Y. Ueda, B. Ivanov, F. Nori, and M. Fiebig, Spin Oscillations in Antiferromagnetic NiO Triggered by Circularly Polarized Light, Phys. Rev. Lett. **105**, 077402 (2010).

[15] M. Takahara, H. Jinn, S. Wakabayashi, T. Moriyasu, and T. Kohmoto, Observation of coherent acoustic phonons and magnons in an antiferromagnet NiO, Phys. Rev. B **86**, 094301 (2012).

[16] H. Meer, F. Schreiber, C. Schmitt, R. Ramos, E. Saitoh, O. Gomonay, J. Sinova, L. Baldrati, and M. Kläui, Direct imaging of current-induced antiferromagnetic switching revealing a pure thermomagnetoelastic switching mechanism in NiO, Nano Lett. **21**, 114 (2020).

[17] K. Gillmeister, D. Golež, C.-T. Chiang, N. Bittner, Y. Pavlyukh, J. Berakdar, P. Werner, and W. Widdra, Ultrafast coupled charge and spin dynamics in strongly correlated NiO, Nat. Commun. **11**, 4095 (2020).

[18] C. Tzschaschel, K. Otani, R. Iida, T. Shimura, H. Ueda, S. Günther, M. Fiebig, and T. Satoh, Ultrafast optical

excitation of coherent magnons in antiferromagnetic NiO, Phys. Rev. B **95,** 174407 (2017).

[19] P. W. Anderson, Antiferromagnetism. Theory of superexchange interaction, Phys. Rev. **79,** 350 (1950).

[20] J. Kuneš, V. Anisimov, S. Skornyakov, A. Lukoyanov, and D. Vollhardt, NiO: Correlated Band Structure of a Charge-Transfer Insulator, Phys. Rev. Lett. **99,** 156404 (2007).

[21] M. Massey, N. Chen, J. Allen, and R. Merlin, Pressure dependence of two-magnon Raman scattering in NiO, Phys. Rev. B **42,** 8776 (1990).

[22] J. Xu, C. Zhou, M. Jia, D. Shi, C. Liu, H. Chen, G. Chen, G. Zhang, Y. Liang, J. Li, W. Zhang, and Y. Wu, Imaging antiferromagnetic domains in nickel oxide thin films by optical birefringence effect, Phys. Rev. B **100,** 134413 (2019).

[23] F. Keffer and C. Kittel, Theory of antiferromagnetic resonance, Phys. Rev. **85,** 329 (1952).

[24] A. Safin, V. Puliafito, M. Carpentieri, G. Finocchio, S. Nikitov, P. Stremoukhov, A. Kirilyuk, V. Tyberkevych, and A. Slavin, Electrically tunable detector of THz-frequency signals based on an antiferromagnet, Appl. Phys. Lett. **117,** 222411 (2020).

[25] D. Lockwood, M. Cottam, and J. Baskey, One-and two-magnon excitations in NiO, J. Magn. Magn. Mater. **104,** 1053 (1992).

[26] J. Milano, L. Steren, and M. Grimsditch, Effect of Dipolar Interaction on the Antiferromagnetic Resonance Spectra of NiO, Phys. Rev. Lett. **93,** 077601 (2004).

[27] H. Qiu, L. Zhou, C. Zhang, J. Wu, Y. Tian, S. Cheng, S. Mi, H. Zhao, Q. Zhang, D. Wu, B. Jin, J. Chen, and P. Wu, Ultrafast spin current generated from an antiferromagnet, Nat. Phys. **17,** 388 (2021).

[28] Y. Wang, P. Deorani, X. Qiu, J. H. Kwon, and H. Yang, Determination of intrinsic spin Hall angle in Pt, Appl. Phys. Lett. **105,** 152412 (2014).

[29] Y. Yang, R. B. Wilson, J. Gorchon, C.-H. Lambert, S. Salahuddin, and J. Bokor, Ultrafast magnetization reversal by picosecond electrical pulses, Sci. Adv. **3,** e1603117 (2017).

[30] W. X. Lim and R. Singh, Universal behaviour of high-Q Fano resonances in metamaterials: terahertz to near-infrared regime, Nano Convergence **5,** 5 (2018).

[31] Z. Wang, G. Dong, S. Yuan, L. Chen, X. Wu, and X. Zhang, Voltage-actuated thermally tunable on-chip terahertz filters based on a whispering gallery mode resonator, Opt. Lett. **44,** 4670 (2019).

[32] A. Kumar, M. Gupta, P. Pitchappa, T. C. Tan, U. Chattopadhyay, G. Ducournau, N. Wang, Y. Chong, and R. Singh, Active ultrahigh-Q $(0.2 \times 10^6)$ THz topological cavities on a chip, Adv. Mater. **34,** 2202370 (2022).

[33] K. Lee, D.-K. Lee, D. Yang, R. Mishra, D.-J. Kim, S. Liu, Q. Xiong, S. K. Kim, K.-J. Lee, and H. Yang, Superluminal-like magnon propagation in antiferromagnetic NiO at nanoscale distances, Nat. Nanotechnol. **16,** 1337 (2021).

[34] E. Rongione, *et al.*, Emission of coherent THz magnons in an antiferromagnetic insulator triggered by ultrafast spin-phonon interactions, Nat. Commun. **14,** 1818 (2023).